Ceramics International 46 (2020) 24347–24354

Contents lists available at ScienceDirect

Ceramics International

journal homepage: www.elsevier.com/locate/ceramint

Tribological and mechanical behaviour of 45S5 Bioglass®-based compositions containing alumina and strontium

M.S. Araujo[a], J.F. Bartolomé[b,*], S. Mello-Castanho[a]

[a] Nuclear and Energy Research Institute (IPEN), Center of Materials Science and Technology (CCTM), Laboratory of Ceramic and Waste Processing (LaPCeRe), São Paulo/SP, 05508-000, Brazil

[b] Instituto de Ciencia de Materiales de Madrid (ICMM), Consejo Superior de Investigaciones Científicas (CSIC), Madrid, 28049, Spain

ARTICLE INFO

Keywords:
Silicate glasses
Strontium oxide
Wear resistance
Friction coefficient
Mechanical properties

ABSTRACT

Although bioactive glasses have been widely used for the surfaces of orthopaedic and dental implants, its limited mechanical strength, low toughness and wear resistance have prevented their use as load-bearing devices. Considering that even a small variation in the composition of such materials can deeply modify their features, inducing very different physicochemical or mechanical properties, the present research was conducted by modifying the glass network of 45S5 Bioglass® by adding Al_2O_3 and SrO to obtain a highly bioactive glass with improved mechanical and tribological performance for biomedical applications. The addition of 2% Al_2O_3 and 2% SrO produced a dense material with the same elastic modulus as 45S5 (~50 GPa). Moreover, the bending strength increased by 60% and the toughness doubled. The wear rate obtained against steel was found to be three times lower than that of 45S5. From the results, it can be assumed that both alumina and strontium synergistically play crucial roles in the mechanical and tribological properties of these new bioactive glasses.

1. Introduction

Bioactive glasses have proven to be of immense interest in medicine owing to its reliable capacity to repair or replace diseased or damaged bones [1]. However, the inherent limited mechanical properties and low wear resistance of bioactive glasses are still their main drawbacks, limiting their use in applications such as load-bearing devices, despite their excellent bioactivity and bonding strength with bone [2–4].

Because the intrinsic fracture toughness of bioactive glasses is dramatically low, the damage and crack resistance improvement are of prime importance, particularly when applied to the repair of load-bearing bones [5]. Appropriate wear resistance is also crucial for the in vivo osteointegration, fixation and lifetime performance of an implant [6]. Therefore, tribological properties are especially critical for the load-bearing surfaces of orthopaedic and dental implants, where bioactive glasses have been widely used as a coating and also when bulk bioactive glasses are employed in orthopaedic applications [7,8].

Although improving mechanical and tribological properties is critical, many bioactive glasses belong to complex systems, and so completely understanding and optimizing not only the mechanical properties but the overall properties by tailoring the structure and composition is not a simple task, and up to now it is still a matter of debate [2,3]. The present research investigated the mechanical and tribological behaviour of four 45S5-based compositions with low strontium oxide and alumina contents. Several studies have associated strontium with improved mechanical properties, such as flexural strength and elastic modulus [4–7]. Likewise, alumina enhances the mechanical properties by increasing the fracture toughness and hardness [6,8].

In our previous study [9], a new 45S5 Bioglass®-based composition containing both strontium and alumina was proposed. Structural and thermal characterisations were conducted in ^{31}P, ^{27}Al, ^{23}Na and ^{29}Si environments obtained using magic-angle spinning–nuclear magnetic resonance (MAS-NMR). The results revealed that the incorporation of Al_2O_3 as a four-coordinated form is essential for optimizing the influence of SrO in the system. The modifications significantly changed the thermal stability, amplifying the working window. Even though many derived bioactive glasses containing strontium and alumina have been investigated. Also, there is a lack of data on the mechanical performance and wear resistance of these silicate glasses.

2. Materials and methods

2.1. Sample preparation

Four Bioglass®-based compositions containing Al_2O_3 and SrO were

* Corresponding author.
E-mail address: jbartolo@icmm.csic.es (J.F. Bartolomé).

https://doi.org/10.1016/j.ceramint.2020.06.216
Received 24 March 2020; Received in revised form 8 June 2020; Accepted 18 June 2020
Available online 25 June 2020

Table 1
Nominal chemical composition (mol%).

Composition	SiO_2	P_2O_5	Na_2O	CaO	Al_2O_3	SrO
BioH	46.1	2.6	24.4	26.9	-	-
BioAl	44.1	2.6	24.4	26.9	2.0	-
BioSr	45.2	2.5	23.9	26.4	-	2.0
BioAlSr	43.2	2.5	23.9	26.4	2.0	2.0

calculated in a molar base, as presented in Table 1. A sample of Bioglass® 45S5 (BioH) composition was also made for comparative purposes. The glasses were prepared from reagent-grade SiO_2 (99.0 wt%; Ventec, Brazil), CaO (99.0 wt%, Casa Americana, Brazil), Na_2CO_3 (95.0 wt%, Casa Americana, Brazil), Al_2O_3 (99.0 wt% Casa Americana, Brazil), $Ca(H_2PO_4)\cdot 2H_2O$ (99.0 wt%, Casa Americana, Brazil) and $Sr(NO_3)_2$ (99.0 wt%, Ventec, Brazil). Batches of 30 g were obtained by homogenising the raw materials in an agate mortar for 10 min and subsequently melting them in a Pt-5%Au crucible at 1500 °C for 1 h in a vertical electric furnace. The glasses were cast into parallelepipedal bars (40 × 15 × 5 mm) and cylindrical (40 mm × Ø15 mm) moulds and annealed at 500 °C for 2 h. They were then slowly cooled to room temperature to remove thermal strain. The batches were cut, ground and polished as required for measurement of the mechanical and tribological properties. Details of the power mixtures processing, sintering parameters and microstructural characterization are reported elsewhere [9]. The densities of the samples were determined by Archimedes' principle with deionised water as the immersion liquid at room temperature.

2.2. Flexural strength and elastic modulus

Five specimens of each composition were subjected to a biaxial flexural strength test in a universal testing machine (Shimadzu Auto Graph AG-X5kN, Japan). The biaxial flexural strength was measured using the piston-on-3-ball method according to the international standard ISO 6872 [10]. Steel balls with diameters of 3.2 mm located every 120° on the circumference of a circle 10 mm in diameter were used for the support. The head was of a flat stylet type with a diameter of 1.2 mm. The tests were performed at room temperature at a crosshead speed of 0.5 mm/min. Samples 15 mm in diameter with thicknesses between 1.3 and 1.5 mm were used for this method.

The bending flexural strength and Young's modulus were measured on a three-point bending test at room temperature using the same testing machine as that used for biaxial strength determination but with an inner span of 30 mm and a crosshead speed of 0.5 m/min. Prismatic samples 40 mm long, 4 mm thick and 12 mm wide were used for the tests. The tensile faces of all specimens (five bars for each composition) were worn with silicon carbide sandpaper and polished with a ceria suspension to less than 1 μm (Struers, RotoPol-22), and the edges were chamfered (~45°) to avoid the influence of microcracks on the mechanical results. The elastic modulus was calculated from the slopes of the load-deflection curves. The formulas, calculation procedures and equipment configuration details used in both the flexural strength and three-point bending tests are described in previous publications [11,12].

2.3. Vickers hardness (HV) and fracture toughness (K_{IC})

The Vickers hardness (HV) of the specimens was determined by microindentation (Buehler model Micromet 5103, Germany) on samples 5 mm thick with surfaces polished to less than 1 μm with a ceria suspension, applying a load of 25 g with an indentation time of 10 s. Fifty Vickers impressions were carried out for each tested sample. The indentation diagonal lengths were measured using an optical microscope. The Vickers indentation fracture was selected to evaluate the fracture toughness (K_{IC}). The indentation and measurement techniques were the same as those for HV; however, the load utilised was 50 g and the lengths of the radial cracks were measured instead of diagonals. The formula is given by Miranzo and Moya [13]. The fracture toughness variation and statistical analysis among each set of samples were evaluated by calculating the cumulative probability and the Weibull modulus (m). The formulas are given by Gong [14].

2.4. Wear test set-up and conditions

A "ball-on-disk"-type wear test was performed using a tribometer (Microtest MT/60/NI, Microtest S.A., Madrid, Spain) in conformity with ASTM G99, in which the glass samples were slid against a stainless-steel ball 6 mm in diameter. For all samples, the applied normal load (F_N) was 3 N, corresponding to an initial Hertzian contact pressure of 0.21 GPa. The test duration corresponded to 1000 m, with a rotation of 180 rpm and a radius of 4.25 mm in unlubricated conditions. At least three sliding wear tests were conducted for each composition. Before each test, the samples were rinsed ultrasonically in acetone and then dried at 90 °C for 30 min. After each sliding test, the worn surfaces were cleared by blowing them with pressurised air before observations. All experiments were carried out under the same conditions, in laboratory air at room temperature, with an average relative humidity of 50 ± 5%. The specific wear rate, W, was calculated by using Eq. (1).

$$W = \frac{\Delta V}{F_N \cdot S} \quad (1)$$

where ΔV is the volume loss after the tests (mm^3), F_N is the applied load (N) and S is the sliding distance (m). To estimate the volume losses, the track profiles were analysed with a surface profilometer (Talysurf CLI 500, Taylor Hobson, Leicester, UK) that maps the measured area by tip-sample surface contact, using a step of 0.01 μm and a scanning speed 0.1 mm/s. A profilometer was used to determine three-dimensional surface topographic maps, so track volumes were estimated, and hence Eq. (1) could be applied. The wear scars were also examined by scanning electron microscopy (SEM; TM3000, Hitachi High-Technologies Co., Tokyo, Japan) at 15 kV of accelerating voltage. Chemical characterisation was performed by energy dispersive X-ray spectroscopy (EDX), which used a silicon-drift detector (SDD) of 30 mm^2 and a resolution of 135 eV (QUANTAX 70 system). The acquisition time for EDX was 200 s for a line scan of 300 μm.

2.5. Raman spectroscopy

Raman spectroscopy was carried out using a micro-Raman spectrometer (WITEC, Confocal Raman Microscope Alpha300 R). The samples were excited by the 532 nm line of an Ar^+ laser and recorded with a microscope objective 50 × /0.7 at 60 s integration time with 45 mW power. The spectra were collected in slices 3 mm thick.

3. Results and discussion

3.1. Mechanical properties

Table 2 summarises the measured density (ρ), biaxial flexural (σ_F) and bending (σ_B) strengths, hardness (HV) and elastic modulus (E). The experimental density for BioH was 2.6920 g/cm^3, which is close to the

Table 2
Mechanical properties of samples BioH, BioAl, BioSr and BioAlSr.

Composition	ρ, g/cm^3	σ_F, MPa	σ_B, MPa	HV, GPa	E, GPa
BioH	2.6920	81 ± 9	50 ± 3	3.6 ± 0.3	50 ± 1
BioAl	2.6948	79 ± 8	68 ± 2	3.8 ± 0.3	48 ± 2
BioSr	2.7108	97 ± 8	75 ± 5	4.4 ± 0.2	51 ± 2
BioAlSr	2.7661	109 ± 8	80 ± 5	4.7 ± 0.3	50 ± 2

reported data (~2.702 g/cm^3) [15]. Like BioH, BioAl presented a density of 2.6948 g/cm^3 instead of the increase observed by other authors [16,17]. This is due to the replacement of silicon by aluminium, which have similar atomic weights, 28.085 and 26.981 g mol^{-1}, respectively. Furthermore, especially in this composition, alumina acted as a former oxide, i.e., in tetrahedral form, and so it effectively replaced the silica in the glass network, as already discussed in our previous work [9]. There was also a clear increase in the density of the BioSr and BioAlSr samples. As expected, owing to its large atomic ratio (~2.45 Å), the addition of strontium to the vitreous network led to an increase in density [15,18]. However, although the density of BioSr was 2.7108 g/cm^3, that of BioAlSr was 2.7661 g/cm^3. This difference, even with the same content, was probably owing to the fact that Sr ions occupied distinct positions in the network, as discussed above.

The elastic modulus (E) of silicate glasses is directly linked to their composition, usually by increasing the alkali cation concentration, and thus a decrease in E is observed. In contrast, metal oxide additions such as SrO can contribute to an increase in E [19–21]. Because the concentration of the modifications was small, all the samples presented similar elastic moduli, around 50 GPa, which conforms to the results of other studies of samples with similar compositions [22,23]. Even though Al_2O_3 acted as a former oxide in BioAl, its presence caused depolymerisation of the silica network, weakening bonds and increasing surface tension. This is mainly due to the replacement of silica with alumina, which is known to make stronger bonds. Thus, it is not expected that alumina, in this particular case, will improve mechanical properties such as fracture toughness and hardness, as pointed out by other authors [6,8,17].

The HV values obtained for BioH and BioAl were similar, 3.6 and 3.8 GPa, respectively, which might be explained by the weakening bonding strength in the glass network. No changes were expected because replacing silica with Al_2O_3 decreased some bonding strength on the atomic scale. Also, an increase in HV usually relates to higher compactness of the glass network with strong bonding strength [24]. In contrast, in the BioSr sample, although the composition resulted in depolymerisation of the network, the incorporation of SrO favoured compactness of the network, thus increasing HV up to 20%. Similarly, with BioAlSr, despite having a different network configuration because of the presence of both Al_2O_3 and SrO, HV varied from 3.6 to 4.7 GPa, indicating an increase of 30%.

The obtained data for all fifty K_{IC} measurements, including minimum and maximum values, were arranged for cumulative distribution function and Weibull analysis. The statistical results of all measurement data, i.e., minimum (K_{ICmin}), maximum (K_{ICmax}), arithmetic average (K_{ICav}), standard deviation and Weibull parameters, are summarised in Table 3. The cumulative distribution was constructed by normalising the data by their average and then ordering the values from the lowest to the highest, taking into account the fact that the cumulative probability of failure (P_i) corresponded to the ith position in the rank of K_{IC}/K_{ICav} and given by (i – 0,5)/50 [14]. The Weibull parameters, K_0 (characteristic toughness) and m (Weibull modulus), were estimated by considering the scale factor, i.e., the probability at 63% and the slope of the fitting curve of each sample, respectively.

The average of K_{IC} values for the four samples varied from 0.18 to 0.38 MPa m$^{1/2}$ for BioH and BioAlSr, respectively. Similar to HV, the

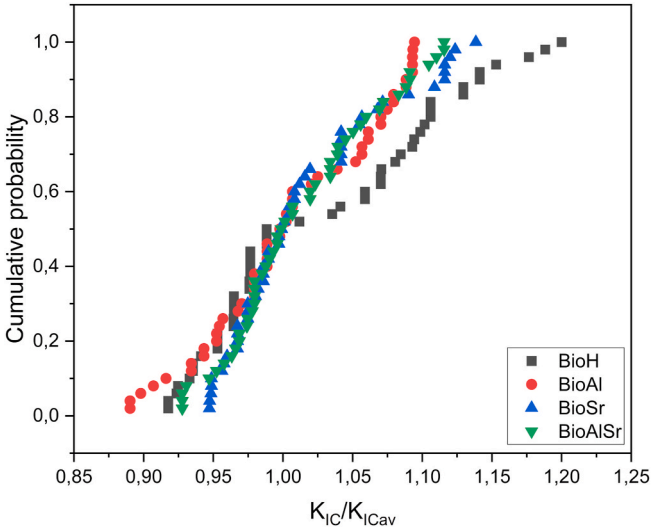

Fig. 1. Cumulative distribution function for normalised toughness of all the glasses.

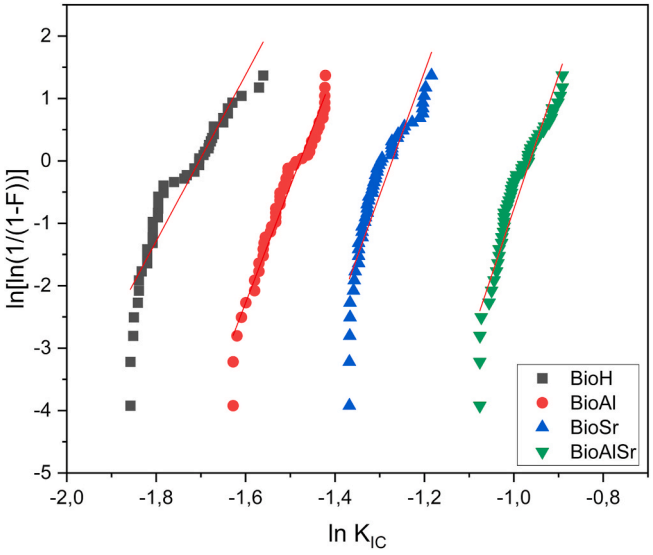

Fig. 2. Weibull plots for the indentation toughness of all glasses.

K_{ICav} values for BioH and BioAl were similar. The K_{IC} value for the BioSr sample increased to 0.27 MPa m$^{1/2}$ and that of BioAlSr was found to be double that of BioH, 0.38 MPa m$^{1/2}$. The coefficient of variation for K_{Ic} fluctuated between 5 and 11%, in agreement in magnitude with other glasses such as soda-lime, which are typically around 10% [14]. Although the results found for K_{Ic} were still lower than those of other commercial glass or glass-ceramics with enhanced toughness, such as Biosilicate® (≈1.0 MPa m$^{1/2}$) and Bioverit® (0.5–2.0 MPa m$^{1/2}$), they are substantial in terms of the main goal of this study, which was to improve the mechanical properties without changing the beneficial

Table 3
Statistical results for the measured indentation toughness of samples BioH, BioAl, BioSr and BioAlSr for indentation load of 50 g.

Composition	Indentation toughness, K_{IC} (MPa m$^{1/2}$)				Weibull parameters	
	Minimum K_{ICmin}	Maximum K_{ICmax}	Average K_{ICav}	Standard deviation	K_0 (MPa m$^{1/2}$)	m
BioH	0.16	0.21	0.17	0.02	0.18	13.3
BioAl	0.20	0.24	0.22	0.01	0.23	18.7
BioSr	0.25	0.31	0.27	0.01	0.27	19.7
BioAlSr	0.34	0.41	0.37	0.02	0.38	21.4

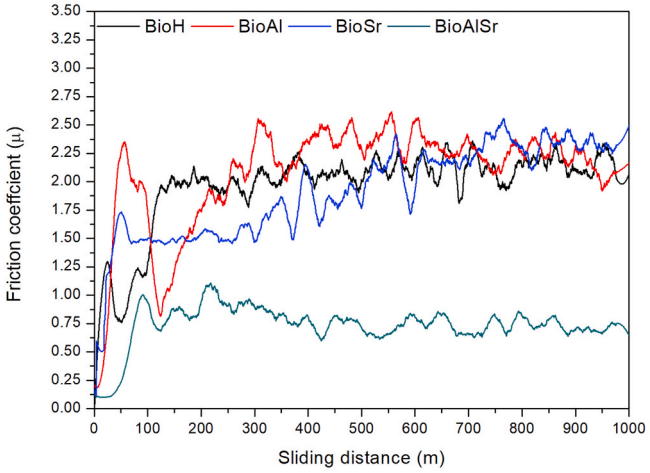

Fig. 3. Friction coefficient as function of sliding distance for samples sliding at 0.02 m/s under a 3 N contact load against a stainless-steel ball.

Table 4
Volume loss (ΔV), friction coefficient (μ) and wear rate (W) after wear tests under 3 N load against stainless steel ball.

	Friction coefficient (μ)	ΔV (mm^3)	W (mm^3/N·m)
BioH	2.1	0.16	5.4×10^{-5}
BioAl	2.2	0.16	5.4×10^{-5}
BioSr	2.1	0.16	5.2×10^{-5}
BioAlSr	0.8	0.09	2.2×10^{-5}

characteristics of BioH (45S5) and also considering bulk samples without any thermal, surface treatment or second-phase reinforcements such as biopolymers, biometals, bioceramics, or carbon materials [25–27].

The cumulative distributions reported in Fig. 1 indicate the same trend for all compositions, in conformity with other glasses from the literature [14,28,29]. The Weibull probability plots in Fig. 2 for all four compositions indicate a linear trend. However, deviations from linearity can be observed more clearly for BioH, which presented a lower *m*, 13.3. For BioAl and BioSr, the *m* values were 18.7 and 19.7, respectively. BioAlSr presented a higher *m*, 21.4. Comparing the results, we can assume that despite the fact that BioH possesses a Weibull modulus similar to that of a soda-lime glass ($m = 13$) [14], considered a homogenous material, higher values for this modulus such as for BioAlSr ($m = 21.4$), could be associated with a material with even higher homogeneity.

3.2. Tribological behaviour

It is important to point out that the information on the wear performance of bioglasses is still scarce. Li et al. [26] reported the first use of graphene nanoplatelets (GNPs) to enhance the wear resistance of 45S5 against an alumina ball. In our study, wear resistance (*W*) against a stainless-steel ball was evaluated. Different plots corresponding to the friction coefficient as a function of distance for each material registered for a 3 N contact load are shown in Fig. 3. All samples tested exhibit similar behaviour: the friction coefficient increases rapidly through the first few metres, and the test proceeds, the initial roughness strongly decreases and the friction coefficient stabilises. This behaviour can be attributed to the polishing effect during the outset of the wear test [30,31]. Still, the coefficient changed significantly according to the sample, which varied from 0.8 to 2.2. After the initial stage, the coefficient of the BioAlSr sample was fixed at 0.8, almost three times lower than the rest of the samples (≈ 2.1).

Table 4 shows that the friction coefficient (μ) reached a steady-state, and data were generated from the three-dimensional (3D) profiles of the tested surfaces, such as the volume loss (ΔV) and calculated wear rate (*W*). The smallest wear track volume loss was measured for the BioAlSr sample, with a *W* value of 2.2×10^{-5}, which was found to be triple the wear resistance of BioH. Fig. 4(a–d) show the surface topographies of the 3D wear tracks for all samples obtained. As expected, the variations in friction coefficient and wear rate generated different

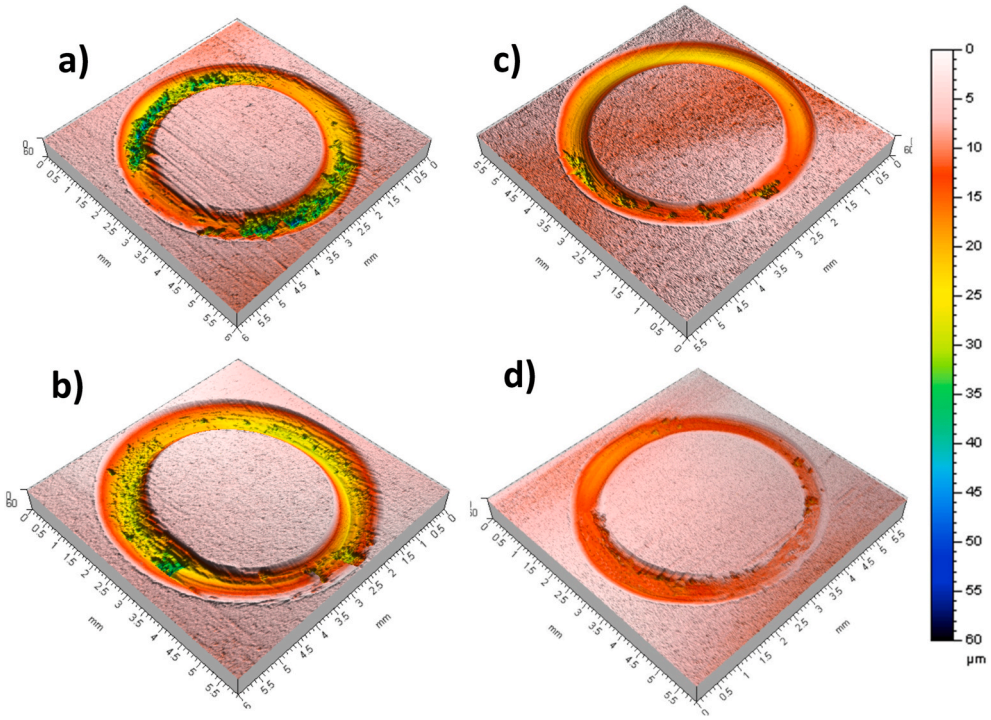

Fig. 4. Representative 3D final wear track topographies corresponding to BioH (a), BioAl (b), BioSr (c) and BioAlSr (d) as a function of depth (coloured scale) under a contact load of 3 N against a steel ball.

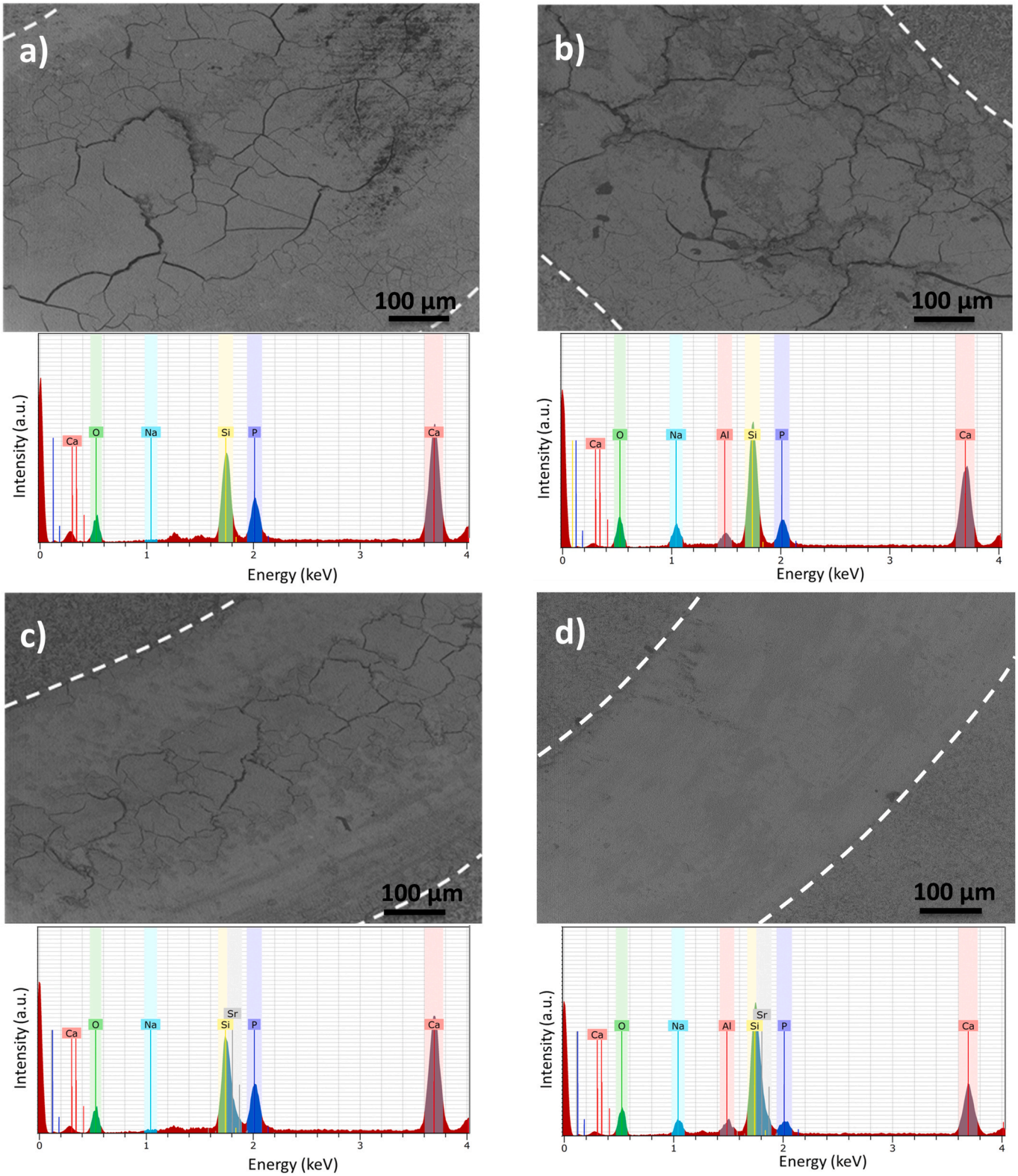

Fig. 5. Representative SEM micrographs of the worn surface and EDX spectra of BioH (a), BioAl (b), BioSr (c) and BioAlSr (d) after sliding against a steel ball under a normal load of 3 N. Dashed lines are added to indicate the borders of the wear track for a better view.

wear tracks. The reduced wear rate and friction coefficients of BioAlSr resulted in the smaller width and depth in its 3D profiles.

Further examinations of wear morphology provided more information regarding the different rates observed. Fig. 5(a–d) show SEM micrographs corresponding to the worn surfaces of all samples tested. Additionally, SEM-EDX representative analysis was performed, and the results are presented below each SEM image. SEM-EDX analysis of all samples, as expected, showed the elements foreseen for each composition. The intensity was fixed for comparative purposes. Each sample exhibited a different peak intensity owing to changes in composition.

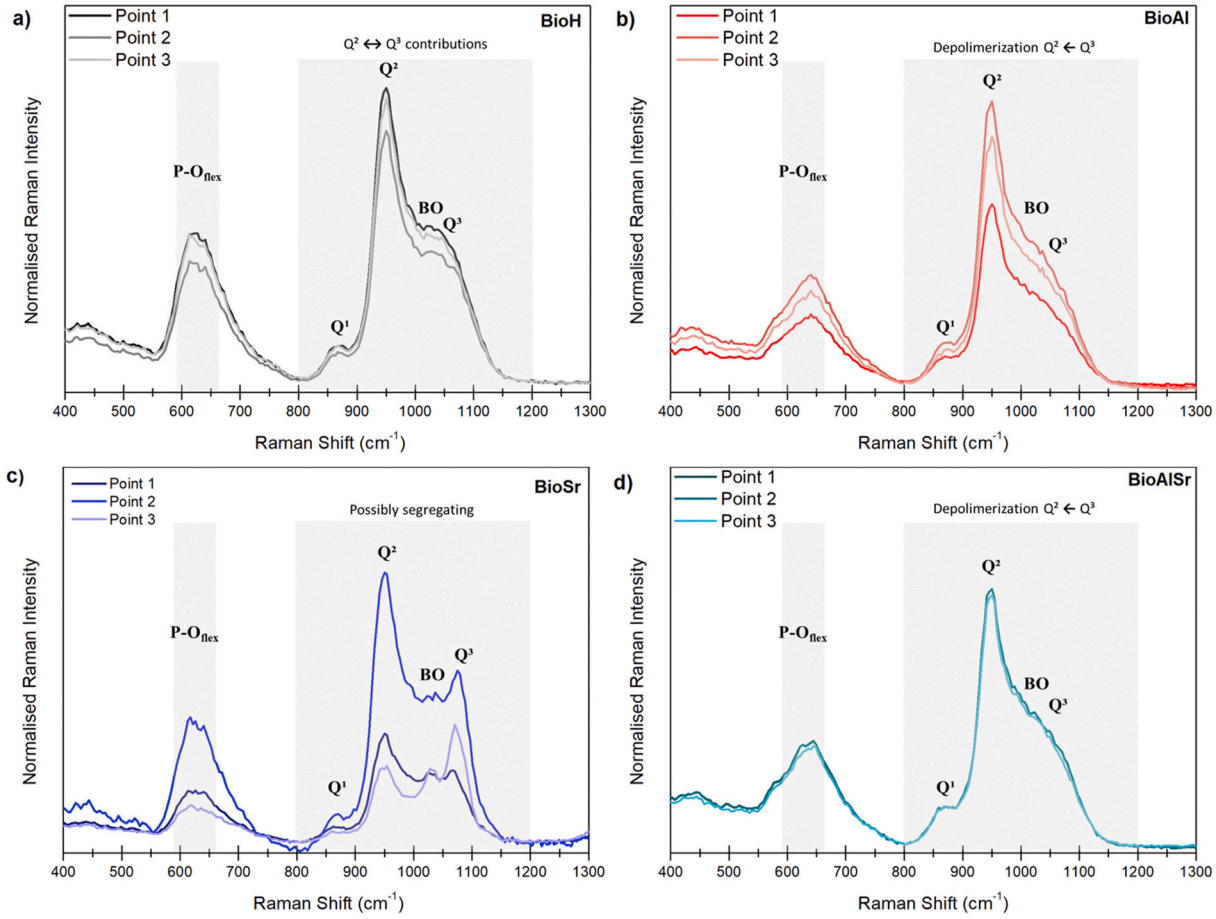

Fig. 6. Three-point Raman spectra collected from BioH (a), BioAl (b), BioSr (c) and BioAlSr (d).

Relevant differences in intensity were noted, where BioH and BioSr exhibited higher values for the calcium and phosphorous peaks, whereas BioAl and BioAlSr exhibited lower values.

After the test at a load of 3 N and an initial mean Hertzian contact pressure of 0.21 GPa, the BioAlSr sample showed a relatively smooth track characteristic of abrasive wear (Fig. 5d), whereas BioH under the same conditions was generally rough and with noticeable evidence of cracking and pull-out. This morphology can be clearly observed in Fig. 5a, where the material removal is dominant. The BioAl and BioSr samples have friction coefficients and wear rates similar to those of BioH. However, it seems that in the case of BioSr, the strontium content contributed to a slight decrease in crack propagation associated with its higher K_{IC} (Table 2) in comparison to BioH and BioAl.

In a recent work by Li et al. [26], it was found that by adding 0.5 wt % graphene oxide (GO) to the 45S5 bioglass, the fracture toughness of the sintered pellets increased by 130.2%, whereas the friction coefficient and specific wear rate decreased by 21.3% and 62.0%, respectively. In our work, the fracture toughness of the BioAlSr sample increased by 109%, whereas the friction coefficient and specific wear rate decreased by 62% and 61%, respectively, without the incorporation of a reinforced second phase.

In this particular case, it can be assumed that the changes in composition foreseen in this study successfully changed the arrangement of the glass network and promoted both alumina and strontium oxide to act in a synergetic way, thus playing a crucial role in the remarkable improvement of the tribological and mechanical performance. To connect and substantiate the structural changes reflected in the glass surface as seen in the tribological behaviour, Raman spectroscopy was conducted.

3.3. Raman spectroscopy

Raman spectroscopy is a useful tool to acquire structural information in the short- and medium-range of the glass surface. The differences observed not only in the Raman spectra but also in other properties through solid-state NMR spectroscopy (discussed elsewhere [9]) associated with the results in mechanical properties and tribological behaviour presented in the previous section contributed to the ponderations contained in this work.

The Raman spectra collected at three points of each sample are presented in Fig. 6(a–d). Excluding BioSr, all samples presented similar spectra at all points collected. The spectra show four principal bands: at (I) 620 cm^{-1}, as P-O$_f$ flexion, (II) 864 cm^{-1}, related to Q^0 units, (III) 944 cm^{-1}, from Q^2 units and (IV) a wide band from 1000 to 1100 cm^{-1}, where we have contributions of ^{0}O-P-O$^-$ stretching of the P_2O_5 sheet unit at 1008 cm^{-1}, asymmetric stretching of bridged oxygen (BO) in all Q species at 1044 cm^{-1}, and symmetric stretching of Q^3 units at 1086 cm^{-1}. In agreement with many works, Q^2 units dominate the open network. However, we can observe a reduction in the range between 1000 and 1100 cm^{-1} for BioAl and BioAlSr, resulting in an increase in Q^2 units at 944 cm^{-1} and consequently an increase in a depolymerised network. Apart from this, no significant changes were observed.

In contrast in BioSr, the three spectra collected were different. At Point 1, the spectra show a significant loss in intensity of the 944 cm^{-1} band. Point 2 presents spectra close to those of other samples. Point 3 is similar to Point 2 but less intense. Therefore, we can assume that the surface is not homogeneous and that Sr ions probably segregate into clusters preferentially associated with the phosphate phase [32]. This trend was confirmed by NMR analysis and Raman deconvolution presented previously [9], which is different from that of the Sr ion

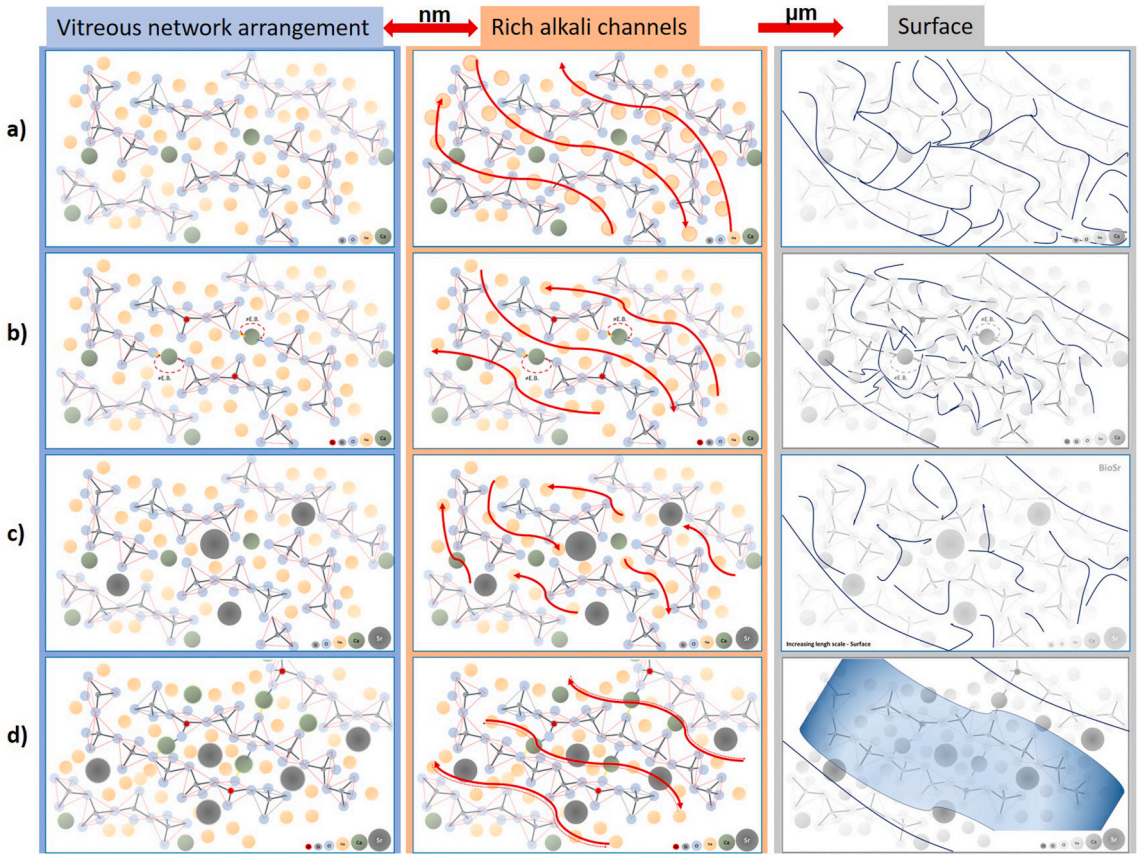

Fig. 7. Schematic representation of glass structure modifications and its implications on surface of a) BioH, b) BioAl, c) BioSr and d) BioAlSr.

contribution in BioAlSr, where new bonds are created as a modifier and may lead to charge balancing through modifier-chain bonding [32], which can contribute to a more resistant and dense material [33].

From these results, it is possible to predict, understand and rationalise the response mechanisms to the mechanical and tribological tests. Fig. 7(a–d) show schematic representations increasing the length scales of the modified glass networks for better understanding. It is important to point out that we are not proposing a mechanism of motion of dislocations or defects, which does not exist in glasses. However, the rearrangement of randomness by the addition of other oxides could affect important configurations on deformation and crack propagation. For all compositions, we are assuming the formation of alkali-rich channels distributed through the glass network [34–36]. These modifier channels are well established by molecular dynamics simulations and experimental studies, and they have important implications in properties that require ionic transport, such as dissolution. In this work, we are extending and extrapolating this concept to the surface by considering the response of the samples to tension such as in the wear test.

Fig. 7a provides a scheme of BioH at the atomic scale, first representing its typical open network, Q^2 distribution, by oxygens mostly coordinated by two silicon. The scheme then shows its rich alkali channels represented by red arrows, which on a large scale, owing to the lack of a mechanism for deformation and the smaller bond energy, will preferably start a crack from the atomic scale to the surface without any barrier. In the BioAl scheme, shown in Fig. 7b, despite the presence of alumina, the behaviour will be similar because the silica was replaced with Al, causing charge decompensation and forming weaker bonds. The tension near the aluminium tetrahedra will create more cracking phenomena in this zone. Differences start to emerge in BioSr, as shown by the scheme in Fig. 7c, where strontium ions act as impurities and contribute to blocking crack propagation because of its verified segregation and atomic size.

Finally, the scheme for BioAlSr, Fig. 7d, shows the combined effect of alumina and strontium oxide on the glass structure. In this particular case, the strontium is continuously distributed at the alkali-rich channels, acting similar to calcium before the substitution. Now, because calcium is required to charge compensate the aluminium tetrahedra, strontium substitutes for calcium in the channels. The presence of strontium in the channels is associated with the increase in Q^2 species (less interconnected network), and the chelating effect of calcium between the chains will contribute to a denser material. The sum of these effects will result in a network with stronger channels. There will still be brittle fracture; however, big changes between samples should be noticed, as the wear tests indicated.

Investigations upon in vitro biological and chemical evaluation are being performed. In addition to the enhanced mechanical properties observed in this work, it is expected that a design combining two oxides – alumina and strontium – could emphasise the material's bioactivity without affecting its stability and degradation rate, thus achieving a new biofunctional material with improved mechanical and tribological properties for regenerative medicine applications.

4. Conclusions

In this work, the mechanical and tribological evaluation of 45S5 Bioglass®-based compositions containing alumina and strontium revealed that both oxides in a synergetic way play a crucial role in the crack and wear resistance of this new modified composition of bioactive glass. The toughness value for BioAlSr was two times higher than that observed in Bioglass®. Moreover, the wear resistance obtained against steel was found to be three times higher in the modified glass than in Bioglass®. Therefore, this new family of bioactive glass has an optimal combination of properties (mechanical and tribological), which opens up the possibility of using these materials in a wide range of

orthopaedic, dentistry and other hard tissue replacement applications where biofunctional and structural properties are required.

Declaration of competing interest

The authors declare that they have no known competing financial interests or personal relationships that could have appeared to influence the work reported in this paper.

Acknowledgements

This research was performed with support from Brazilian government through their respective funding agencies CAPES (CsF/PDSE-Project No 88881.189953/2018-01), CNPq (GD-Project No 142172/2016-2, Universal Research Project No 481260/2012-9 and PD. 312135/2016-5) and FAPESP (Project No 1999/01924-2).

References

[1] M. Saini, Implant biomaterials: a comprehensive review, World J. Clin. Cases 3 (2015) 52.
[2] K. Januchta, M. Stepniewska, L.R. Jensen, Y. Zhang, M.A.J. Somers, M. Bauchy, Y. Yue, M.M. Smedskjaer, Breaking the limit of micro-ductility in oxide glasses, Adv. Sci. 6 (18) (2019) 1901281.
[3] L. Souza, J.H. Lopes, D. Encarnação, I.O. Mazali, R.A. Martin, J.A. Camilli, C.A. Bertran, Comprehensive in vitro and in vivo studies of novel melt-derived Nb-substituted 45S5 bioglass reveal its enhanced bioactive properties for bone healing, Sci. Rep. 8 (1) (2018) 1–15.
[4] A. Goel, R.R. Rajagopal, J.M.F. Ferreira, Influence of strontium on structure, sintering and biodegradation behaviour of CaO–MgO–SrO–SiO_2–P_2O_5–CaF_2 glasses, Acta Biomater. 7 (11) (2011) 4071–4080.
[5] D. Bellucci, A. Sola, R. Salvatori, A. Anesi, L. Chiarini, V. Cannillo, Role of magnesium oxide and strontium oxide as modifiers in silicate-based bioactive glasses: effects on thermal behaviour, mechanical properties and in-vitro bioactivity, Mater. Sci. Eng. C 72 (2017) 566–575.
[6] H. Tripathi, C. Rath, A. Sampath, P. Pratim, Structural , physico-mechanical and in-vitro bioactivity studies on SiO_2-CaO-P_2O_5-SrO-Al_2O_3 bioactive glasses, Mater. Sci. Eng. C 94 (2019) 279–290.
[7] S.K. Arepalli, H. Tripathi, S.K. Hira, P.P. Manna, R. Pyare, S.P. Singh, Enhanced bioactivity, biocompatibility and mechanical behavior of strontium substituted bioactive glasses, Mater. Sci. Eng. C 69 (2016) 108–116.
[8] H. Liu, R. Yang, Y. Wang, S. Liu, Influence of alumina additions on the physical and chemical properties of lithium-iron-phosphate glasses, Phys. Procedia 48 (2013) 17–22.
[9] M.S. Araujo, A.C. Silva, J.F. Bartolomé, S. Mello-Castanho, Structural and thermal behavior of 45S5 Bioglass®-based compositions containing alumina and strontium, J. Am. Ceram. Soc. (2020) 17061 jace.
[10] International Organization for Standardization, ISO 6872, Dentistry - Ceramic Materials, 3th ed., (2008).
[11] A. Smirnov, J.F. Bartolomé, Mechanical properties and fatigue life of ZrO_2 – Ta composites prepared by hot pressing, J. Eur. Ceram. Soc. 32 (2012) 3899–3904.
[12] A. Smirnov, J.F. Bartolomé, Microstructure and mechanical properties of ZrO_2 ceramics toughened by 5 – 20 vol % Ta metallic particles fabricated by pressureless sintering, Ceram. Int. 40 (2014) 1829–1834.
[13] P. Miranzo, J.S. Moya, Elastic/plastic indentation in ceramics: a fracture toughness determination method, Ceram. Int. 10 (1984) 147–152.
[14] J. Gong, Indentation toughness of ceramics: a statistical analysis, Ceram. Int. 28 (2002) 767–772.
[15] Y. Xiang, J. Du, Effect of strontium substitution on the structure of 45S5 bioglasses, Chem. Mater. 23 (2011) 2703–2717.
[16] H. Tripathi, S. Kumar, A. Sampath, U. Gupta, Structural characterization and in vitro bioactivity assessment of SiO_2–CaO–P_2O_5–K_2O–Al_2O_3 glass as bioactive ceramic material, Ceram. Int. 41 (9) (2015) 11756–11769.
[17] R.K. Brow, Nature of alumina in phosphate glass: I, properties of sodium aluminophosphate glass, J. Am. Ceram. Soc. 76 (1993) 913–918.
[18] J.K. Christie, N.H. de Leeuw, Effect of strontium inclusion on the bioactivity of phosphate-based glasses, J. Mater. Sci. 52 (2017) 9014–9022.
[19] A.K. Srivastava, R. Pyare, S.P. Singh, Elastic properties of substituted 45S5 bioactive glasses and glass-ceramics, Int. J. Sci. Eng. Res. 3 (2012).
[20] C.-C. Lin, L.-C. Huang, P. Shen, $Na_2CaSi_2O_6$–P_2O_5 based bioactive glasses. Part 1: elasticity and structure, J. Non-Cryst. Solids 351 (2005) 3195–3203.
[21] A.K. Varshneya, Fundamentals of Inorganic Glasses, Elsevier, 1994.
[22] L.L. Hench, Bioceramics, J. Am. Ceram. Soc. 81 (2005) 1705–1728.
[23] L.L. Hench, An Introduction to Bioceramics, second ed., Imperial College Press, 2013.
[24] P. Jha, K. Singh, Effect of MgO on bioactivity, hardness, structural and optical properties of SiO_2–K_2O–CaO–MgO glasses, Ceram. Int. 42 (2016) 436–444.
[25] F. Baino, J. Barberi, E. Fiume, G. Orlygsson, J. Massera, E. Verné, Robocasting of bioactive SiO_2 -P_2O_5-CaO-MgO-Na_2O-K_2O glass scaffolds, J. Healthc. Eng. 2019 (2019) 78–88.
[26] Z. Li, N.W. Khun, X. Tang, E. Liu, K. Aik, Mechanical , tribological and biological properties of novel 45S5 Bioglass s composites reinforced with in situ reduced graphene oxide, J. Mech. Behav. Biomed. Mater. 65 (2017) 77–89.
[27] M. Rizwan, M. Hamdi, W.J. Basirun, Bioglass® 45S5-based composites for bone tissue engineering and functional applications, J. Biomed. Mater. Res. 105 (2017) 3197–3223.
[28] G. Kaur, O.P. Pandey, K. Singh, D. Homa, B. Scott, G. Pickrell, A review of bioactive glasses: their structure, properties, fabrication, and apatite formation, J. Biomed. Mater. Res. 102 (2013) 254–274.
[29] G. Kaur, V. Kumar, F. Baino, J.C. Mauro, G. Pickrell, I. Evans, O. Bretcanu, Mechanical properties of bioactive glasses, ceramics, glass-ceramics and composites: state-of-the-art review and future challenges, Mater. Sci. Eng. C 104 (2019) 109895, https://doi.org/10.1016/j.msec.2019.109895.
[30] K. Kameo, K. Friedrich, J.F. Bartolomé, M. Díaz, S. López-Esteban, J.S. Moya, Sliding wear of ceramics and cermets against steel, J. Eur. Ceram. Soc. 23 (2003) 2867–2877.
[31] T. Rodriguez-Suarez, J.F. Bartolomé, A. Smirnov, S. Lopez-Esteban, R. Torrecillas, J.S. Moya, Sliding wear behaviour of alumina/nickel nanocomposites processed by a conventional sintering route, J. Eur. Ceram. Soc. 31 (2011) 1389–1395.
[32] J.K. Christie, R.I. Ainsworth, N.H. de Leeuw, Investigating structural features which control the dissolution of bioactive phosphate glasses: beyond the network connectivity, J. Non-Cryst. Solids 432 (2016) 31–34.
[33] J.K. Christie, R.I. Ainsworth, D. Di Tommaso, N.H. De Leeuw, Nanoscale chains control the solubility of phosphate glasses for biomedical applications, J. Phys. Chem. B 117 (2013) 10652–10657.
[34] G.N. Greaves, EXAFS and the structure of glass, J. Non-Cryst. Solids 71 (1985) 203–217.
[35] G.N. Greaves, W. Smith, E. Giulotto, E. Pantos, Local structure, microstructure and glass properties, J. Non-Cryst. Solids 222 (1997) 13–24.
[36] A.C. Da Silva, Structure and percolation of bioglasses, Adv. Struct. Mater., Springer, Cham, 2016, pp. 49–84.